

# Photon emission from melanoma cells during brief stimulation by patterned magnetic fields: is the source coupled to rotational diffusion within the membrane?

Blake T. Dotta<sup>1</sup>, Robert M. Lafrenie<sup>1,2,3</sup>, Lukasz M. Karbowski<sup>1</sup> and Michael A. Persinger<sup>1</sup>

<sup>1</sup> *Biomolecular Sciences Program, Laurentian University, Sudbury, Ontario, P3E 2C6, Canada*

<sup>2</sup> *Regional Cancer Program, Health Sciences North, Ontario, P3E 5J1, Canada*

<sup>3</sup> *Northern Ontario School of Medicine, Sudbury, Ontario, P3E 2C6, Canada*

**Abstract.** If parameters for lateral diffusion of lipids within membranes are macroscopic metaphors of the angular magnetic moment of the Bohr magneton then the energy emission should be within the visible wavelength for applied  $\sim 1 \mu\text{T}$  magnetic fields. Single or paired digital photomultiplier tubes (PMTs) were placed near dishes of  $\sim 1$  million B16 mouse melanoma cells that had been removed from incubation. In very dark conditions ( $10^{-11} \text{ W/m}^2$ ) different averaged (RMS) intensities between 5 nT and 3.5  $\mu\text{T}$  were applied randomly in 4 min increments. Numbers of photons were recorded directly over or beside the cell dishes by PMTs placed in pairs within various planes. Spectral analyses were completed for photon power density. The peak photon emissions occurred around 1  $\mu\text{T}$  as predicted by the equation. Spectra analyses showed reliable discrete peaks between 0.9 and 1.8  $\mu\text{T}$  but not for lesser or greater intensities; these peak frequencies corresponded to the energy difference of the orbital-spin magnetic moment of the electron within the applied range of magnetic field intensities and the standard solution for Rydberg atoms. Numbers of photons from cooling cells can be modified by applying specific intensities of temporally patterned magnetic fields. There may be a type of “cellular” magnetic moment that, when stimulated by intensity-tuned magnetic fields, results in photon emissions whose peak frequencies reflect predicted energies for fundamental orbital/spin properties of the electron and atomic aggregates with large principal quantum numbers.

**Key words:** Photon emissions — Melanoma cells — Magnetic fields — Spectral analyses — Intensity-tuning

**Abbreviations:** FM, frequency modulated; LED, light emitting diode; LTP, long term potentiation; PMT, photomultiplier tube; RMS, root mean squared.

## Introduction

The interactions between applied weak intensity magnetic fields and plasma cell membranes have been explored by multiple models that emphasize direct forces such as Lorenz effects (Adey 1981; Engstrom and Fitzsimmons 1999; Weaver et al. 1999), resonance processes (Ludwig 1968; Lednev 1991;

Liboff 1992; Mulligan et al. 2012), or challenges to the kT boundary (Bini and Rubin 2007; Cifra et al. 2011). The components of the membrane most frequently emphasized have been the distribution of charges, alterations in the capacity of the polar groups of proteins composing ion channels, and the liquid crystal states of the lipid components (Lenaz 1987). In the pursuit of the mechanism by which photons are emitted during slow depolarization from cancer and normal cells after removal from incubation, we examined the potential validity of a model and mechanism that involves the release of photon energy from the interaction between components of the membrane that could display circumferential move-

---

Correspondence to: Michael A. Persinger, Biomolecular Sciences Program, Laurentian University, Sudbury, Ontario, P3E 2C6, Canada

E-mail: mpersinger@laurentian.ca

ments and the application of specific, weak rotating magnetic fields. Here we present data to support this possibility.

Within the last two decades there has been a re-examination of the role of “mitogenic” radiation that was enthusiastically pursued during the 1930s (Quickenden 1974; Popp et al. 1988). There are several reviews of ultraweak photon emissions that are coupled to the cell’s function (Isojima et al. 1995) and intercellular communication (Sun et al. 2010). Recently we completed a series of experiments showing that cells from many normal and aberrant cell lines, removed from incubation, emit photons during the subsequent approximately 10 hours (Dotta et al. 2011a, 2011b). The estimated numbers of photons measured by photomultiplier tubes (PMTs) indicated that the losses occur in increments of energy in the order  $10^{-20}$  J as the cell membrane slowly depolarizes (Dotta et al. 2011a). This “quantum” of energy is the same order of magnitude as that associated with action potentials in axons, the separation of potassium ions that maintain the resting plasma membrane potential, forces applied over distances occupied by covalent and hydrogen bonds, and the sequestering of ligands to receptors (Persinger 2010).

Movement in a closed path, such as a circle or even certain fractal configurations, has potential properties to interact with applied magnetic fields. Technically velocity within a circle is accelerating. Circumferential movements, as manifested by the lateral diffusion of lipids within the plasma cell membrane, have been inferred by a variety of methods (Lenaz 1987; Furtula et al. 1990). The diffusion coefficients (D) of selected lipids, such as the mobile lipophilic quinones involved with electron transfer, range from  $10^{-6}$  cm<sup>2</sup>/s (Lenaz 1987) to  $3 \times 10^{-9}$  cm<sup>2</sup>/s (Furtula et al. 1990). The equivalent diffusion length  $(4Dt)^{1/2}$ , where t is time, in one second would be between  $2 \times 10^{-5}$  m/s to  $5.5 \times 10^{-7}$  m/s. Lenaz (1987) suggested the slower diffusions occur over longer linear distances because the lipids are obstructed by the proteins dispersed within the phospholipid matrices. Asymmetrical soma geometry would also affect the coefficients for this “smooth” rotation.

This continuous movement over a bound surface could be considered a condition analogous to the magnetic moment (Am<sup>2</sup>) of the orbit of an electron around an atom. In traditional expression:

$$\mu = e p / (2m) \quad (1)$$

where  $\mu$  is the magnetic moment, e and m indicate the unit charge and mass of the electron and p is the angular momentum. The orbital magnetic moment of the electron for the Bohr magneton is in the order of  $10^{-24}$  Am<sup>2</sup>.

When applied to the cell the “magnetic moment” would be the product of angular velocity (m/s)/m divided by the cell radius, moment of inertia (kgm<sup>2</sup>) and the unit charge (As) divided by mass (kg). For estimates for the “rotating

components with charge<sup>e</sup> for the cell membrane we assumed the slowest diffusion rates, between  $10^{-7}$  to  $10^{-8}$  m/s (Lenaz 1987; Persinger 2010), which were divided by cell radius. Assuming a radius of between 7.5 and 12.5  $\mu$ m to accommodate the range for most melanoma cells (Ochalek et al. 1988) and the density of water, the mass of each cell would range from 1.8 to  $8.2 \times 10^{-12}$  kg.

The resulting cellular “magnetic moments” would be between  $10^{-23}$  and  $10^{-24}$  kgm<sup>2</sup>/s. We assumed there would be a central tendency, given the expected heterogeneity of velocities of lateral diffusion, within more or less normally distributed dispersions. When multiplied by the unit charge ( $1.6 \times 10^{-19}$  As) and divided by the mass of an electron  $9.11 \times 10^{-31}$  kg, the median “cellular” magnetic moment is within the  $10^{-23}$  Am<sup>2</sup> or J/T. If a magnetic field with the appropriate cell-coupled frequency were applied with an intensity of  $\sim 1$   $\mu$ T ( $10^{-6}$  T), the resulting energy would be within the range of  $10^{-19}$  J.

This domain of quanta of energy is within visible wavelength that could be detected by PMTs. The intensity also results in a peak frequency of  $\sim 16$  to 18 Hz when applied to the discrepancy between an electron’s orbital and spin magnetic moments. This frequency is remarkably congruent with solutions for Rydberg atoms. These excited atoms display at least one electron with very high principal quantum numbers and exhibit amplified responses to applied electric and magnetic fields. Here we present data to support these possibilities.

## Materials and Methods

### Preparation of cells

B16-BL6 mouse melanoma cell cultures were maintained in  $150 \times 20$  mm tissue culture plates (Sarstedt, Laval, Qc) in Dulbecco’s Modified Essential Medium (DMEM, Hyclone, Logan, UT) accompanied with 10% fetal bovine serum, 100  $\mu$ g/ml of streptomycin and 100 U penicillin/ml (Invitrogen, Burlington, ONT). Cells were incubated at 37°C in 5% CO<sub>2</sub>. The cell monolayers were harvested by incubation in 0.25% trypsin-EDTA, collected by centrifugation, and seeded onto 6.0 cm by 1.5 cm tissue plates to a final count ( $\sim 10^6$  cells/plate). The cells were then removed from the incubator and transported to the biophysics laboratory.

### Magnetic field equipment and exposure

Our laboratory has developed a technology for computer-generating patterned magnetic fields with basic temporal parameters that simulate many cellular processes (Persinger 2003). Depending upon programming, one can generate any theoretical or simulated physiological pattern. The magnetic

fields in this study were generated by converting a row of numbers between 1 and 256 to incremental voltages between  $-5$  and  $+5$  V employing complex software, where  $127=0$ , that we have described previously (Persinger 2003). The series of numbers generated a specific pattern that was frequency-modulated and has been shown to increase analgesia in rodents (Martin et al. 2004) and invertebrates (Thomas et al. 1997). The same pattern modifies biomolecular pathways (Buckner 2011) and alters T-type calcium channel conduction in cancer cells but not normal cells (Buckner et al. 2013). The shape of this frequency-modulated sequence is shown in Figure 1. This pattern was also instrumental as the second stage for the establishment of a brief ( $\sim 8$  min) entanglement between distant loci of experimentally-induced bursts of photons from the simultaneous injection of hydrogen peroxide into plates containing small volumes of sodium hypochlorite (Dotta and Persinger 2012).

The DOS-based computer software was programmable and allowed the specification of numbers of cycles (repetitions of the pattern), the duration of each number or voltage (point duration), the time between cycles (interpattern interval), and the amplitude (intensity) of the output. The optimal computer is a 286 Zenith because of its stability of internal timing, although any computer can be functional if the variable processing speeds from Windows and intrinsic circuitry are stabilized by a small software program. In this study, the duration of each point, that is the time a given voltage was presented for each point ( $n = 849$ ) that composed the patterned magnetic field application, was 3 ms. This discrete voltage for this duration was presented to a pair of the application solenoids. This value was selected because previous research had shown its efficiency for slowing cancer cell growth (Karbowski et al. 2012) and affecting physiological responses coupled to overt behaviour (Whissell and Persinger 2007). This precision is important. Point durations that are less (1 ms, 2 ms) or greater (4 ms, 5 ms, 10 ms) produce less analgesic effect in rodents (Martin et al. 2004), do not delay the growth of several types of cancer cells (Buckner 2011), and do not facilitate the influx of  $\text{Ca}^{2+}$  through T-type channels (Buckner et al 2013).

The discrete voltage values were converted from the range of numbers by a custom constructed digital-to-analogue converter. It delivered the discrete value to one of four pairs of solenoids contained within the boxes. Consequently, a magnetic field was generated at any given time between the two opposing solenoids using reed relays (Radioshack Compact 5VDC/1A SPST Reed relays; Model 275-232, 260  $\Omega$ ,  $\sim 50$  m copper wire). The four solenoids were arranged in a "circle" within each of the two 5 cm by 8.5 cm boxes. The circumference of the "circle" of solenoids was about 15 cm. A built-in commutator successively activated a pair of solenoids every 0.5 s. Consequently, the time required for all four pairs of solenoids to be activated before the circular

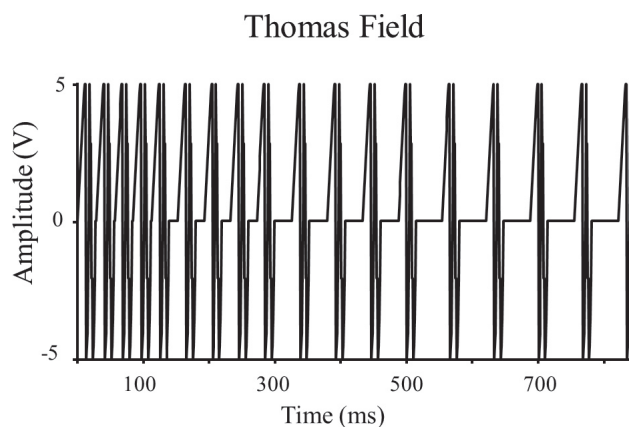


**Figure 1.** Pattern of the frequency-modulated field (Thomas field) primarily employed in the experiments.

"rotation" was complete was 2 s. The plane of the rotation was perpendicular to the plane upon which the tissue plates were placed. The layer of cells at the bottom of the dishes was also normal to the rotational plane.

The two boxes were separated by 10 to 11 cm. Direct measurements by power meters with input to laptop computers and verification of the pattern through commercial, calibrated telephone hookup solenoids coupled to audio-amplifiers indicated that the programmable range of mean intensities of the applied field in the space occupied by the cells varied from an average RMS of 5 nT to 3.5  $\mu\text{T}$ . We selected this range because it included and extended below and above the intensities of the field that were predicted by the ("membrane magnetic moment") model to enhance photon emissions.

Two standard plastic dishes (5 cm wide, 1 cm deep) each containing  $\sim 1$  million melanoma cells in 5 cc of fluid were stacked between the two boxes. The superimposed (2) plates of cells were employed because direct measurements indicated more spontaneous photon emissions. The distance between the  $\sim 0.2$  cc fluid containing the layer of cells in one plate and the one below (or above) was 1.4 cm. The cells and the exposure equipment were housed within an industrial acoustic chamber that was also a Faraday cage. The computers that controlled the generation of the magnetic field and measured the PMTs were housed outside of the room. Magnetometers (FVM-400 Vector, MacIntyre Electric Design Associates) indicated that the resultant geomagnetic field intensity within the chamber where the cell dishes were placed was  $\sim 26,000$  nT compared to the typical 45,000 nT outside of the chamber.

#### *Exposure procedure and PMT measurements*

During our pilot studies with digital photon units (Sens Tech LTD DM0090C; spectral response range 280 nm to

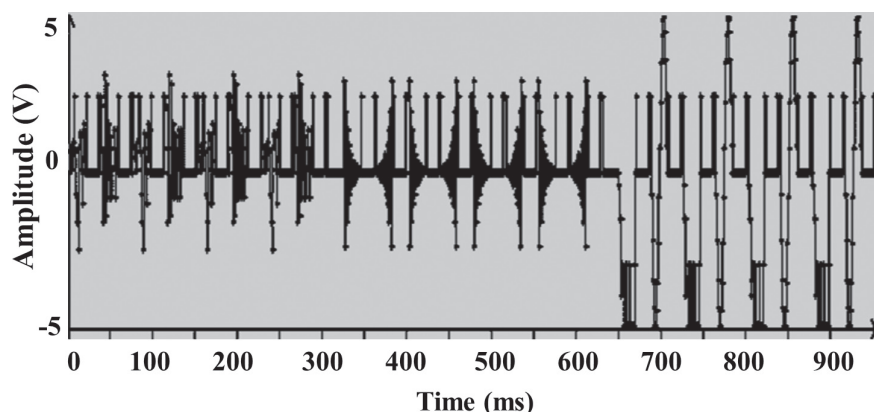


**Figure 2.** Pattern of the complex sequenced pre-exposure field employed in the experiments.

850 nm, peak sensitivity around 370 nm) involving about 60 different samples and 10 different days over several weeks to establish appropriate parameters we found that the photon emissions were most reliable when the ambient background photon levels were above  $\sim 400$  counts *per* 20 ms. Assuming  $10^{-19}$  J *per* photon,  $2 \times 10^4$  photons/s and the aperture of the photomultiplier tube (2.1 cm), this threshold was calculated to be about  $10^{-11}$  W/m<sup>2</sup>.

When the chamber was darkened extensively by black terry cloth over the windows and complete removal of ambient external light (counts < 100 photons *per* 20 ms; background measures in the chamber during the maximum darkness were between 4000 and 5000 photons/s) the phenomena described in this study were not observed. We could also produce the phenomena by adding light from a rectified (green) LED in the chamber that elevated the background to above 400 counts *per* 20 ms. All measurements were recorded by Lenovo laptops (Windows 7) that were maintained outside the chamber. The text edited by Chang et al. (1998) on the measurement and nature of biophotons was particularly instructive to avoid artifact problems.

During the first part of the experiment that involved about 20 different plates of cells the two apposed plates of cells were placed over the aperture of a single digital photomultiplier tube. The range of delay from the time the cells were removed from the incubator to the time they were exposed and measured ranged between 1.5 and 2 hours. Our previous work, employing analogue PMTs, indicate that biophoton emissions were still copious during this period (Dotta et al. 2011a). After accommodating for numbers of cells and aperture area, the output from each cell *per* s was in the order of  $2$  to  $4 \times 10^{-20}$  J/s according to both digital and analogue instrumentation. This is within the range both measured and theoretically derived from a variety of approaches (Persinger 2010; Dotta et al. 2011a).

For each experiment, a set of plates containing melanoma cells was exposed for  $\sim 4$  min to each of the 10 different intensities of the frequency-modulated field and to the no field condition. There were a total of 6 replicates *per* intensity and for the no field condition (66 samples). Pilot studies indicated that there was an enhancement of the effect if there was a pre-exposure for 2 to 4 min to a complex sequenced magnetic field with an average intensity of  $\sim 3$   $\mu$ T.

This specific complex sequenced magnetic field has been shown to affect cellular differentiation (Persinger et al. 2001; St-Pierre et al. 2003) and repair (Lado and Persinger 2012). The pattern is composed of 10,000 points (discrete voltages between 0 and 256), each presented for 1 ms. The gestalt shape is shown in Figure 2. The individual patterns that composed the complex sequenced field, each presented for 200 ms, are shown in Figure 3. The order was: Burst, LTP, FM, LTP, repeated 4 times, followed by a neutral field, then Positive ring, LTP, Negative ring, LTP presented 4 times, followed by a neutral field, and, then Fibonacci, LTP, 5 Hz, LTP presented four times.

Because of these results all experiments began with this procedure before baseline which was followed by the subsequent counterbalanced order of presentation of the 10 intensities. The numbers of photons *per* 20 ms were recorded by specialized software by the external laptop for 2 complete minutes for each of the intensities. The 20 ms sample time was selected to maximum data collection without obtaining excessive numbers of data points for subsequent spectra analyses.

During the second part of the experiment after the clear display of the non-linear intensity magnetic field effect upon photon emission was replicated multiple times over several months, a paired PMT procedure was instituted. For some experiments two identical digital PMTs each with their own laptops external to the chamber were placed over the top and under the bottom of the plates, perpendicular to this position and the placement of the solenoid boxes,

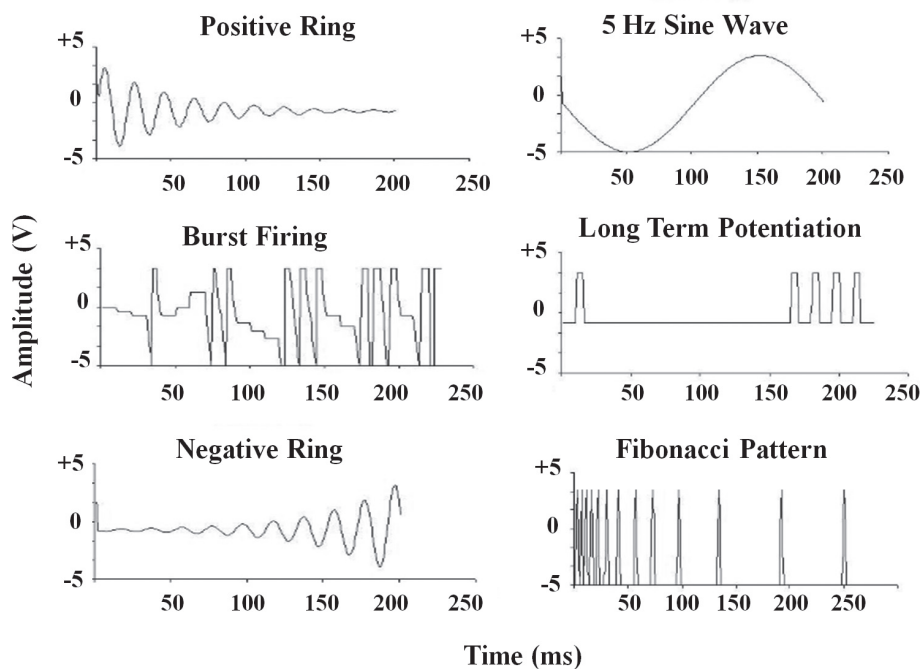


**Figure 3.** The six shapes of the fundamental patterns whose various combinations produced the complex sequenced pre-exposure field. Each point duration (voltage) was 1 ms.

or, asymmetrically such that one was under the cells and the other was perpendicular to the plane of the plates and the solenoid boxes. A diagram of the various orientations is shown in Figure 4. The two PMTs were altered in the different paired positions to minimize instrumental artifact. The same procedure of field exposure was employed. However, the data were sampled in 50 ms increments (20 samples *per s*) in order to visualize the changes more effectively in real time from the laptop because of the nature of the software.

#### Data analyses

In the first part of the experiment, the total numbers of photons *per* 20 ms increment above the mean background for the 2 min sample period for each of the 10 increments of the applied field intensities as well as the no field condition were calculated from the raw data. The means and standard deviations were computed for each of the 6 different experiments for the each intensity. The means and standard deviations for the deviations from the baseline as a function of the intensity of the applied frequency-modulated field were plotted.

Triplicate samples from each of the 2 min PMT samples for each of the different intensities were randomly selected from the data. Spectra analyses were completed by SPSS-PC version 16. These analyses were completed because we

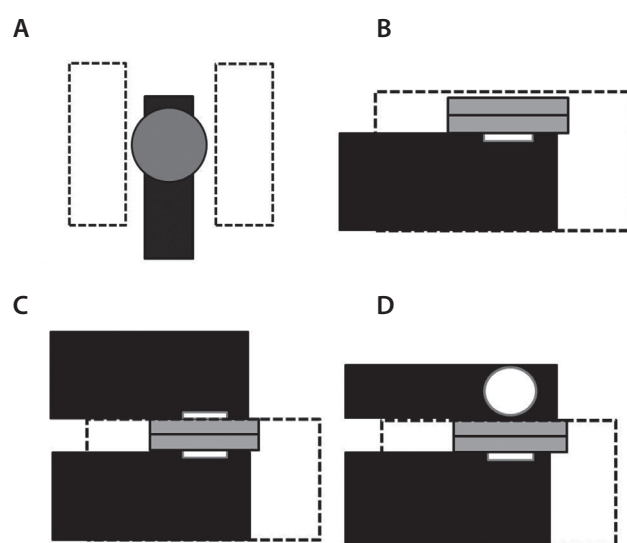


**Figure 4.** Block diagrams of variations in orientations of the PMTs with respect to the double dishes of melanoma cells. Boxes with dotted lines (not to scale) refer to the boxes containing the solenoids, grey figures are the cell dishes, black boxes containing white circles are PMTs with white circles corresponding to the PMT aperture. **A.** Single PMT with double plates sitting on aperture (**B**). **C.** Double PMT with one PMT aperture on top and the other PMT aperture on the bottom of the two plates. **D.** Double PMT with one PMT beneath and the other PMT perpendicular to the plane of the cells. PMT, photomultiplier tube.

had predicted specific peaks in power within the optimal intensity band that would reflect solutions for the Rydberg frequency and the differential energy between the spin and orbital magnetic moments for electrons for the specific range of the applied magnetic fields.

For the second part of the experiment involving the twin (coupled) PMTs, the time-coupled correlations between the total numbers of photon counts *per* unit time for the two measurements were completed for no field and various intensities of the field conditions. The photon counts for the serial 4,400 samples for one PMT were plotted against the 4,400 values for the second PMT. Although the sampling rate for each independent PMT was 20 *per* s (50 ms increments) direct measurements indicated the discrepancy between the two instruments was not more than one temporal increment. Because there was a conspicuous shift in the shape and dispersion of photon numbers when the optimal field strengths were present vs not present, additional analyses were completed for the numbers of photons that exceeded 4.0 standard deviations from the central cluster.

## Results

### *Optimal intensity for photon emissions matches predicted value*

Figure 5 shows the discrepancy in photon counts from background during the first 2 min durations of the different intensities of the magnetic field pattern (samples from the last 2 min of a field exposure produced comparable effects). The maximum photon emissions from the plates of cells occurred when the field strengths were between 0.9 and 1.8  $\mu\text{T}$ . Above 1.8  $\mu\text{T}$  and below 0.9  $\mu\text{T}$  the photon emissions were either inconsistent or minimal and approached that of baseline conditions. The mean peak of 80 photon counts *per* gate time of measurement would correspond to a radiant flux density of roughly  $1.4 \times 10^{-11} \text{ W/m}^2$ . This value was obtained by multiplying the numbers of photons *per* gate (80 photons/ $\Delta t$ ) by: 1) the number of gates *per* second (50  $\Delta t/s$ ), 2) the average energy value of a single photon at 630 nm ( $3.6 \times 10^{-19} \text{ J/photon}$ ) and 3) the width of the active diameter of the PMT's photocathode ( $10^4 \text{ cm}^2/\text{m}^2$ ). In this instance the conventional symbol  $\Delta t$  corresponds to the sampling window, or the gate time of measurement. The wavelength 630 nm was selected as an average because it is the median spectral response range of the PMT. This increase of  $1.4 \times 10^{-11} \text{ W/m}^2$  was superimposed upon the background baseline of  $\sim 400$  photons *per* gate. This background level of  $\sim 400$  photons *per* gate has a corresponding flux density of  $\sim 7 \times 10^{-11} \text{ W/m}^2$  (assuming the energy of a photon at 630 nm), which was the approximate limen to produce the effect.

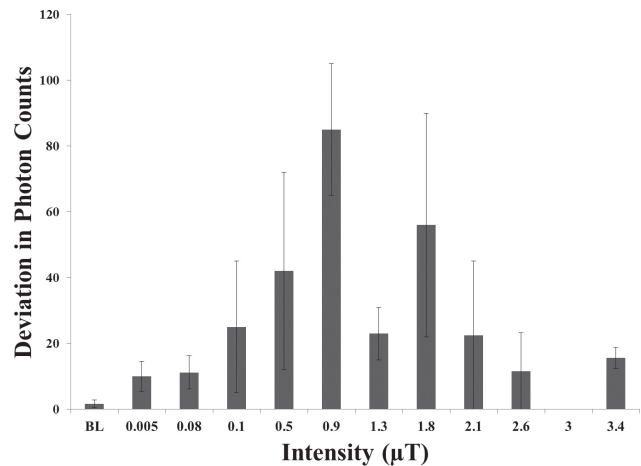


**Figure 5.** Deviation from baseline of numbers of photons *per* 20 ms increment from the cells exposed to the various intensities (RMS) in nT to  $\mu\text{T}$  of the patterned magnetic field shown in Figure 1. Vertical bars indicated standard deviations.

### *Spectral analyses*

Representative results of the spectra analyses (Fourier transform) of each trial for sample intensities are shown in Figure 6. For all triplicates from the each intensity there were reliable peaks of power within the photon spectra within the equivalent of  $\sim 20 \text{ Hz}$  (the tallest peak on the right in Figure 6) and two smaller peaks at 9.65 Hz and 10.37 Hz frequency for the 0.9  $\mu\text{T}$  to 1.8  $\mu\text{T}$  intensity fields only. These frequencies were never present when the applied intensity of the field was below 0.9  $\mu\text{T}$  or 3.0  $\mu\text{T}$  or above. We included the 2.6  $\mu\text{T}$  in the figure because it displayed this pattern once.

The intrinsic structure of the primary spectral peak (20 Hz) is shown in Figure 7A for two of the intensities within the range of optimal intensities. The increased power displayed a normal-like distribution with a slow rise starting around 19.95 Hz, a peak between 20.05 Hz and 20.15 Hz and a slow decline until about 20.25 Hz. In comparison, the dark thick horizontal line at the base represents the values for this band for cells exposed to lesser or greater intensities. The secondary double peaks around 10 Hz also displayed a narrow band (Figure 7B).

### *Double PMT simultaneous correlational patterns*

Figure 8 shows the correlational configurations (scatterplots) between the two PMTs placed at different orientations when the optimal strength magnetic field was either absent or present. The vertical and horizontal axes represent standardized values. Figure 8A is representative of the relationship between photons generated from the two plates of cells when the PMTs were above the top dish and below the bottom dish

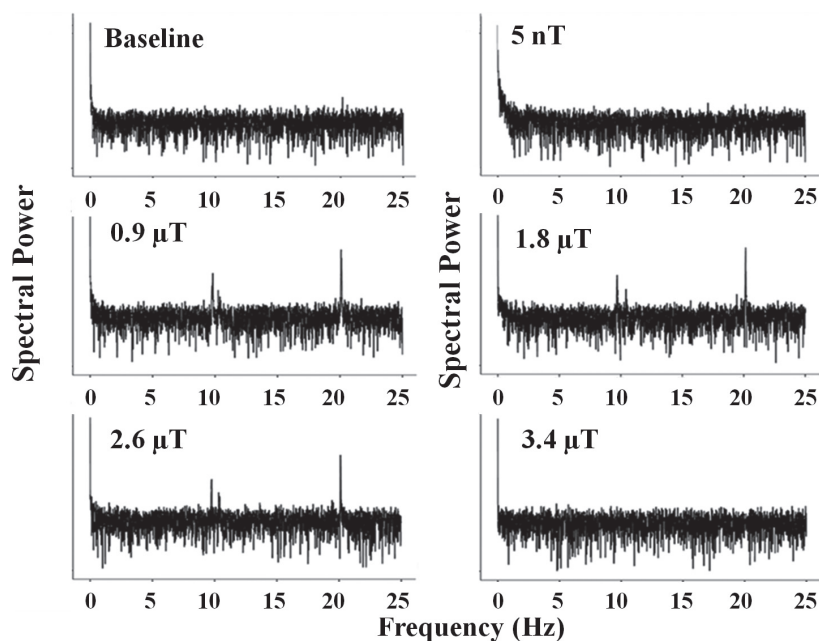


**Figure 6.** Spectral analyses (Fourier transform) of raw photon counts *per* 20 ms increment for 120 s from samples of cells that had been exposed to the various intensities of the applied frequency-modulated magnetic fields. Vertical axes indicate relative power while the horizontal axis indicated intrinsic frequency based upon the unit (20 ms). The emergence of the large sharp peak around 20 Hz and the two small peaks around 10 to 12 Hz only emerged with the intensities calculated by the model.

(Figure 4C). The shape on the left is when no field is present. The shape on the right is when optimal field strength was applied (0.9–1.8  $\mu\text{T}$ ). It is important to note that magnetic fields alone had no discernable effect upon these PMTs. In addition, the same experiments performed with a plate of cell culture media only produced no effects. These effects were observed only when cells were present.

Figure 8B shows the relationship in numbers of photons between the two PMTs when the optimal field was being applied to the cell dishes. The more vertically distorted shape on the left reflects the association between two PMTs orthogonal to each other (Figure 4D) while the one of the right shows the temporal association between photon outputs when the two PMTs are parallel (one top, one bottom) to each other (Figure 4C). Switching the two PMTs to the different positions did not alter this effect.

The median range of increased peaks (spikes) in photons *per* 50 ms was between 6 and 8 *per* 2 min interval when the optimal field strength was present. This was equivalent to about 1 spike every 15 to 20 s. On the other hand, when there was no field present the typical numbers of spikes were between 0 and 2 *per* 2 min interval.

On the bases of the shapes of the scattergrams and quantitative values for numbers of photons for the different orientations we inferred that the presence of the optimal intensity field elongated and constricted the shape of the “photon fields” being emitted from the double layer of cells. A picture, not to scale, of how this might appear with optimal measurement is shown in Figure 9. The two horizontal grey boxes represent the cell dishes, the solid lines depict the no-field condition and the dotted lines indicate the alteration in

the shape of the “photon field” when the magnetic field was applied parallel to the surface of the plates (and cell layer) while the generated field rotated through the perpendicular plane. This elongation and constriction was not present in control conditions.

## Discussion and Conclusion

One approach to Life, as cogently articulated by both Bohr (1958) and Schrödinger (1944), is that, at the macroscopic level, living systems reflect the fundamental processes of quantum phenomena. Cells emit photons as a component of multiple chemical processes from (very likely) many sources and by various mechanisms. In previous experiments (Dotta et al. 2011a) we found that one major source of photons in cancer and normal cells in culture was the plasma cell membrane after removing of cells from stable incubation and maintaining at room temperatures. The temperature of these cells could potentially affect their viscosity at higher and lower temperatures, but at such temperatures the cells would no longer be viable. The numbers of photons emitted *per* unit time *per* cell was equivalent to about  $10^{-20}$  J/s. This “quantum” is within the order of magnitude and convergent with the coefficients for the energy over distance for the forces between  $\text{K}^+$  charges that maintain the plasma membrane potential (Persinger 2010) and the energy associated with the sequestering of many agonists to receptors.

The movements of components of the cell membrane, particularly classes of lipids and proteins, through this three-

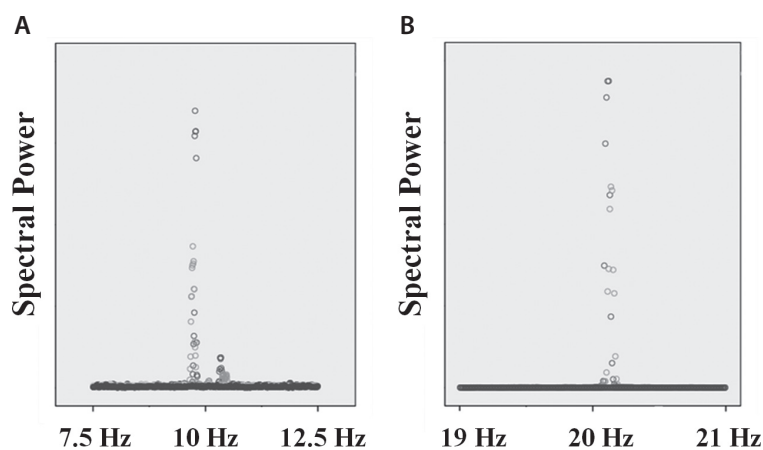


**Figure 7.** **A.** Relative power peaks for the secondary double spikes (9–10 Hz) in photon emission frequency for cells exposed to the 0.9 or 1.8  $\mu\text{T}$  fields. There was no response from the same cells exposed to lower strengths or to those above 2.8  $\mu\text{T}$ . These measures are contained with the thick zero line. **B.** Relative power peaks for the primary spike around 20 Hz for cells exposed to the 0.9  $\mu\text{T}$  or 1.8  $\mu\text{T}$  field.

dimensional shell indicated that this expansive torus might display properties analogous to moving charge-currents. They might be considered a field of point current charges. The physical properties would be similar to (but reflective of the more complex macroscopic level) an electron moving around a proton in the hydrogen atom. The resulting “*membrane magnetic moment*” when exposed to the appropriate intensity from an applied magnetic field would be associated with an energy that might be discerned by measurement of photons. In this experiment the ratio of the applied magnetic field compared to background was  $\sim 1:10$  (applied field strength of  $\sim 2 \mu\text{T}$  with a background of  $26 \mu\text{T}$ ). The ratio of applied to background field intensities may be important and should be investigated.

The results of our experiments strongly suggest that there is moderately strong quantitative accuracy for the model. We assumed the standard range of cell circumferences reported for melanoma cells and the estimated lateral diffusion rates (particularly when accommodating their deviation for symmetrical spheroids). We found a peak in photon emissions within two minutes after application of the predicted intensity of magnetic fields by this model. We are assuming at present that the wide range of the distribution of effective intensities between about 0.5 and occasionally  $2.1 \mu\text{T}$  could represent either different populations of intramembrane components representing the charge or the different geometries of cell shape within different “splits” of cells. The shapes of these melanoma cells were irregular; however, this irregularity is common among all the cells within the dish. These calculations were based upon an average. We suggest that the field intensity range of the responses reflected the different arrays of the shapes of the cells as well.

The non-linearity of the effect also reduces the possibility that the increased photon emissions were artifacts of some anomalous microcurrent induction within the PMTs. The intensity-dependent increase in photon emissions only

required about 4 min of exposure, about the same duration as a single cycle of NAD(P)H oscillations ( $\sim 4.2$  to  $5.5 \text{ mHz}$ ). Rosenspire et al. (2001) showed that pulsed d.c. electric fields could couple to the natural NAD(P)H oscillations in fibrosarcoma cells.

We considered that the functional atomic aggregates associated with the photon emissions from circumferential diffusion of lipids through the membrane might be analogous to or display properties like an excited atom with relatively high principal quantum numbers. Such Rydberg atoms (Dudin and Kuzmich 2012) are known for their amplified response to applied magnetic and electric fields, electron wave functions that approximate classic orbits (including the Bohr magneton) and relatively protracted decay periods. The attenuation of the influence from nuclear protons by the more proximal electrons allows the outer electrons to behave and display properties of the Bohr magneton upon which our model is largely based.

According to the classic Rydberg relation,  $e^2/(4\pi\epsilon_0 r^2) = mv^2/r$ . The solution for frequency ( $\text{s}^{-1}$ ) is  $e^2/(4\pi\epsilon_0 r^2 mv)$ . Assuming a cell radius of  $7.5 \mu\text{m}$  and a lateral diffusion rate of  $10^{-6} \text{ m/s}$  the standing frequency would be  $\sim 18 \text{ Hz}$ . This value is remarkably congruent with the highly reliable spectral peak measured from the photon emission amplitudes (sampled 50 times *per s*) from the melanoma cells measured in our experiments.

Our assumptions had been that lateral diffusion of an optimal population of lipids whose functional groups display Rydberg atomic properties are macrocosmic analogues, but not equivalents, of the two magnetic moments of the electron. The minute but significant difference between the spin moment of  $9.28476 \times 10^{-24} \text{ J/T}$  and the orbital moment of  $9.27408 \times 10^{-24} \text{ J/T}$  for a model electron is  $1.068 \times 10^{-26} \text{ J/T}$ . If  $1 \mu\text{T}$ -fields are applied to this difference, the resulting energy of  $1.068 \times 10^{-32} \text{ J}$ , when divided by Planck’s constant ( $6.624 \times 10^{-34} \text{ Js}$ ), results in a frequency of  $16 \text{ Hz}$ . If the effective field strength was  $\sim 1.3 \mu\text{T}$  (well within the range of

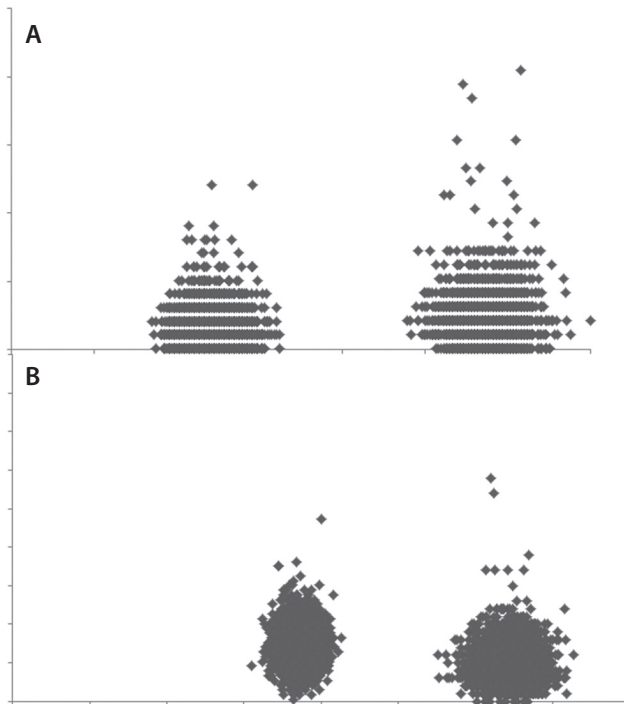


**Figure 8.** **A.** Real-time (50 ms increments) correlations (scatterplots) of photon emissions between the two adjoining PMTs between which the cells were placed. Vertical and horizontal axes correspond to raw photon counts (*per* 50 ms) for PMT1 and PMT2. The plot on the left is the no field condition; plot of the right with the dorsal scatter occurred when the optimal intensity field was applied. **B.** Real time correlations between photon emissions when the optimal fields were present when the two PMTs were perpendicular to each other (left) or apposing (parallel) to each other. PMT, photomultiplier tube.

standard deviation of the variable field intensities for our RMS value of  $0.9 \mu\text{T}$ , the solution would be 20 Hz. Interestingly, several authors have reported enhancement of either tumor growth or weight when magnetic field frequencies between 12 Hz (Bellossi et al. 1988, 1991) and 20 Hz (Babicova et al. 2000, 2004) have been applied to animals.

We approached the interactions between the circumferential component within the cell membrane and the facilitated photon emission by the applied magnetic field as if they were classical electromagnetic processes. This assumes a dipole characteristic of the electromagnetic radiation. However, the cells show a marked departure from spherical symmetry. If the source of the photon emissions could be described as a quadrupole within this non-symmetrical context then energies more typical of gravitational phenomena could be involved. As aptly stated by Puthoff (1989), gravitational potentials share many of the characteristics of van der Waals and Casimir forces more than fundamental Coulomb forces. The Casimir effect is the

interaction between a pair of neutral, parallel conducting planes because of the quantum effects relate to disturbances in the vacuum of the electromagnetic field or the zero-point energy of a quantized field. Recent calculations (Persinger 2012) indicate that specific solutions for electromagnetic and “gravitational” phenomena may converge within the band of the visible wavelength.

Van der Waals forces are prominently present in surface-surface interactions of cells. This may be relevant to our observations because application of the Casimir equation:

$$F = (\pi^2/240) \cdot (hc/a^4) \cdot S \quad (2)$$

where  $F$  is the Casimir force,  $S$  is the area of the surface (of the plate or area of the cell culture),  $a$  is the separation between the two layers (1.4 cm),  $h$  is the modified Planck’s constant, and  $c$  is the velocity of light, results in a force of  $\sim 5 \times 10^{-23}$  N. Applied across the 1.4 cm the force results in an energy of  $9.317 \times 10^{-25}$  J. When divided by Planck’s constant the equivalent frequency is about 1.41 GHz, or within measurement error of interstellar neutral hydrogen (the 21 cm hydrogen line).

The 21 cm wavelength is congruent with the small differences in energy when the angular momentum and energy of the proton-electron rotations shift from parallel to antiparallel configurations. As noted earlier the difference in energy between the spin and orbital electron magnetic moments when applied to strengths of optimal fields employed in this study would be equivalent to the peak in spectral power noted in

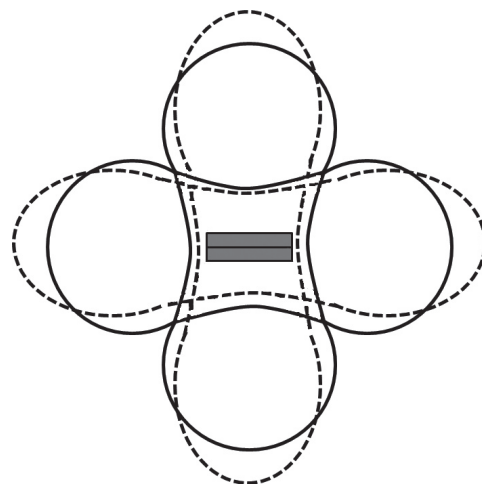


**Figure 9.** Artistic depiction of inferences from the quantitative photon emission data collected by the different angles and orientations of the two PMTs around the double plates of cells. Closed lines indicate shape of “photon field” normally (no field). Dotted lines indicate the “constriction and elongation” of form when the appropriate field intensity was applied.

the photon emissions. Whether or not this is spurious or contributory to what we have observed must still be established.

Although from some perspectives the application of a Casimir potential may be considered to be unlikely, even a remote probability has potential significance. According to Bordag et al. (2001), material boundaries from concentrated external electromagnetic fields polarize the vacuum resulting in creations of real particles from virtual particles (vacuum oscillations) by the transfer of energy. Such “particle creation” occurs only if the boundary condition is a function of time. In the present study the boundary condition of the applied field was changing.

The shift in the spatial distribution of the scattergram during the double PMT measurements reinforces the validity of the effect. As noted in Figure 9, the most parsimonious interpretation of the data patterns we measured would be the presence of a “quadrupole”-like display of photons with the direction of emissions above and below and to each side of the pairs of plates. The application of the rotating field with flux lines along the same plane as the surface of the cells resulted in “constriction” of the field such that more photons protruded outside the boundaries (the solid line in Figure 9). These were detected as the photon spikes that occurred on average every 15 to 20 s when the optimal intensity of fields was present. Given the differences in resting membrane potentials between cancer cells and non-cancer cells it would be interesting to discern if there would be a shift in frequency in visible light that could potentially differentiate cancer cells from non-cancer cells.

**Acknowledgement.** We thank Dr. W. E. Bosarge Jr, CEO of Capital Technologies, Inc. for support. Part of this research was funded by O.G.S. (Ontario Graduate Scholarships).

## References

- Adey W. R. (1981): Tissue interactions with non-ionizing electromagnetic fields. *Physiol. Rev.* **61**, 435–513
- Babincová M., Sourivong P., Leszczynska D., Babinec P. (2000): Influence of alternating magnetic fields on two-dimensional tumor growth. *Electromagnetic Biology and Medicine* **19**, 351–355  
<http://dx.doi.org/10.1081/JBC-100102126>
- Babincová M., Sourivong P., Leszczynska D., Babinec P. (2004): Effects of GSM microwaves, pulsed magnetic field, and temperature on fractal dimension of brain tumors. *Chaos, Solitons and Fractals* **20**, 1041–1045  
<http://dx.doi.org/10.1016/j.chaos.2003.09.020>
- Bellossi A., Desplaces A. (1991): Effect of a 9 mT pulsed magnetic field on C3H/BI female mice with mammary carcinoma. A comparison between the 12 Hz and the 460 Hz frequencies. *In Vivo* **5**, 39–40
- Bellossi A., Desplaces A., Morin R. (1988): Effect of a pulsed magnetic field on tumoral C3H/BI female mice. *Cancer Biochem. Biophys.* **10**, 59–66
- Bini V., Rubin A. (2007): Magnetobiology: the kT paradox and possible solutions. *Electromag. Biol. Med.* **26**, 45–62  
<http://dx.doi.org/10.1080/15368370701205677>
- Bohr N. (1958): *Atomic Physics and Human Knowledge*. N.Y. John Wiley & Sons
- Bordag M., Mohideen U., Mostepanenko V. M. (2001): New developments in the Casimir effect. *Physics Reports* **353**, 1–205  
[http://dx.doi.org/10.1016/S0370-1573\(01\)00015-1](http://dx.doi.org/10.1016/S0370-1573(01)00015-1)
- Buckner C. A. (2011): Effects of electromagnetic fields on biological processes are spatial and temporal-dependent. Laurentian University, Ph.D. Dissertation, Biomolecular Sciences Program
- Buckner C. A., Buckner A. L., Koren S. A., Persinger M. A., Lafrenie R. M. (2013): Exposure to a specific time-varying electromagnetic field inhibits cancer cell growth by affecting calcium influx (in submission)
- Chang J. J., Fisch J., Popp F. A. (1998): *Biophotons*, Kluwer Academic Pub, Dordrecht
- Cifra M., Fields J. Z., Farhadi A. (2011): Electromagnetic cellular interactions. *Prog. Biophys. Mol. Biol.* **105**, 223–246  
<http://dx.doi.org/10.1016/j.pbiomolbio.2010.07.003>
- Dotta B. T., Buckner C. A., Cameron D., Lafrenie R. M., Persinger M. A. (2011a): Biophoton emissions from cell cultures: biochemical evidence for the plasma membrane as the primary source. *Gen. Physiol. Biophys.* **30**, 301–309
- Dotta B. T., Buckner C. A., Lafrenie R. M., Persinger M. A. (2011b): Photon emissions from human brain and cell culture exposed to distally rotating magnetic fields shared by separate light-stimulated brains and cells. *Brain Res.* **388**, 77–88  
<http://dx.doi.org/10.1016/j.brainres.2011.03.001>
- Dotta B. T., Persinger M. A. (2012): „Doubling“ of local photon emissions when two simultaneous, spatially separated, chemiluminescent reactions share the same magnetic field configurations. *J. Biophys. Chem.* **3**, 72–80  
<http://dx.doi.org/10.4236/jbpc.2012.31009>
- Dudin Y. O., Kuzmich A. (2012): Strongly interacting Rydberg excitations of a cold atomic gas. *Science* **336**, 887–889  
<http://dx.doi.org/10.1126/science.1217901>
- Engstrom S., Fitzsimmons R. (1999): Five hypotheses to examine the nature of magnetic field transduction in biological systems. *Bioelectromag.* **30**, 423–440  
[http://dx.doi.org/10.1002/\(SICI\)1521-186X\(199910\)20:7<423::AID-BEM3>3.0.CO;2-W](http://dx.doi.org/10.1002/(SICI)1521-186X(199910)20:7<423::AID-BEM3>3.0.CO;2-W)
- Furtula V., Kahn I. A., Nothnagel E. A. (1990): Selective osmotic effect on diffusion of plasma membrane lipids in maize protoplasts. *Proc. Nat. Acad. Sci. U.S.A.* **87**, 6532–6536  
<http://dx.doi.org/10.1073/pnas.87.17.6532>
- Isojima Y., Isoshima T., Nagai K., Kikuchi K., Nakagawa H. (1995): Ultraweak bioluminescence detected from rat hippocampal slices. *NeuroReport* **6**, 658–660  
<http://dx.doi.org/10.1097/00001756-199503000-00018>
- Karbowska L. M., Harribance S. L., Buckner C. A., Mulligan B. P., Koren S. A., Lafrenie R. M., Persinger M. A. (2012): Digitized quantitative electroencephalographic patterns applied as magnetic fields inhibit melanoma cell proliferation in culture. *Neurosci. Lett.* **523**, 131–134  
<http://dx.doi.org/10.1016/j.neulet.2012.06.059>

- Lado W. E., Persinger M. A. (2012): Spatial memory deficits and their correlations with clusters of shrunken neuronal soma in the cortices and limbic system following a „mild“ mechanical impact to the dorsal skull in female rats. *J. Behav. Brain Sci.* **2**, 333–342  
<http://dx.doi.org/10.4236/jbbs.2012.23038>
- Lednev V. V. (1991): Possible mechanisms for the influence of weak magnetic fields on biological systems. *Bioelectromag.* **12**, 71–75  
<http://dx.doi.org/10.1002/bem.2250120202>
- Lenaz G. (1987): Lipid fluidity and membrane protein dynamics. *Biosci. Rep.* **7**, 823–837  
<http://dx.doi.org/10.1007/BF01119473>
- Liboff A. R. (1992): Cyclotron resonance in membrane transport. In: *Interaction Mechanisms of Low Level Electromagnetic Fields and Systems*. (Eds. B. Norden and C. Ramel), pp. 130–147, Oxford Press, Oxford
- Ludwig H. W. (1968): A hypothesis concerning the absorption mechanisms of atmospheric in the nervous system. *Int. J. Biometeor.* **12**, 93–98  
<http://dx.doi.org/10.1007/BF01553500>
- Martin L. J., Koren S. A., Persinger M. A. (2004): Thermal analgesic effects from weak, complex magnetic fields and pharmacological interactions. *Pharm. Biochem. Behav.* **78**, 217–227  
<http://dx.doi.org/10.1016/j.pbb.2004.03.016>
- Mulligan B. P., Gang N., Parker G. H., Persinger M. A. (2012): Magnetic field intensity/melatonin-molarity interactions: experimental support with planarian (*Dugesia sp.*) activity for a resonance-like process. *Open J. Biophys.* **2**, 137–143  
<http://dx.doi.org/10.4236/ojbiphy.2012.24017>
- Ochalek T., Nordt F. J., Tullberg K., Burger M. M. (1988): Correlation between cell deformability and metastatic potential in B16-F1 melanoma cell variants. *Cancer Res.* **48**, 5124–5128
- Persinger M. A. (2003): Neurobehavioral effects of brief exposures to weak intensity, complex magnetic fields within experimental and clinical settings. In: *Magnetotherapy: Potential Therapeutic Benefits and Adverse Effects*. (Eds. M. J. McLean, S. Engstrom and R. R. Holcomb), pp. 89–118, TFG Press, New York
- Persinger M. A. (2010): 10–20 Joules as a neuromolecular quantum in medicinal chemistry: an alternative approach to myriad molecular pathways. *Cur. Med. Chem.* **17**, 3094–3098  
<http://dx.doi.org/10.2174/092986710791959701>
- Persinger M. A. (2012): Potential origins of a quantitative equivalence between gravity and light. *Open Astron. J.* **4**, 19–25
- Persinger M. A., St-Pierre L. S., Koren S. A. (2001): Geophysical variables and behavior: XCI. Ambulatory behavior in rats following prenatal exposures to complex magnetic field designed to interact with genetic expression. *Percep. Mot. Skil.* **92**, 183–192  
<http://dx.doi.org/10.2466/pms.2001.92.1.183>
- Popp F. A., Li K. H., Mei W. P., Gale M., Neurohr R. (1988): Physical aspects of biophotons. *Experientia* **44**, 576–585  
<http://dx.doi.org/10.1007/BF01953305>
- Puthoff H. E. (1989): Gravity as zero-point-fluctuation force? *Phys. Rev.* **39**, 2333–2342  
<http://dx.doi.org/10.1103/PhysRevA.39.2333>
- Quickenden T. I. (1974): Weak luminescence from yeast *saccharomyces cerevisiae* and the existence of mitogenetic radiation. *Biochem. Biophys. Res. Comm.* **60**, 764–770  
[http://dx.doi.org/10.1016/0006-291X\(74\)90306-4](http://dx.doi.org/10.1016/0006-291X(74)90306-4)
- Rosenspiere A. J., Kindzelskii A. L., Petty H. R. (2001): Pulsed DC electric fields couple to natural NAD(P)H oscillations in HT-1080 fibrosarcoma cells. *J. Cell Sci.* **114**, 1515–1520
- St-Pierre L. S., Persinger M. A. (2003): Conspicuous histomorphological anomalies in the hippocampal formation of rats exposed prenatally to a complex sequenced magnetic field within the nanoTesla range. *Percep. Mot. Skil.* **97**, 1307–1314
- Schrodinger E. (1944): *What is life?* Cambridge Univer. Press, Cambridge
- Sun Y., Wang C., Dai J. (2010): Biophotons as neural communication signals demonstrated by in situ biophoton autography. *Photochem. Photobiol. Sci.* **9**, 315–322  
<http://dx.doi.org/10.1039/b9pp00125e>
- Thomas A. W., Kavaliers M., Prato F. S., Ossenkopp F. A. (1997): Antinociceptive effects of pulsed magnetic fields in the land snail, *Cepaea nemoralis*. *Neurosci. Lett.* **222**, 107–110  
[http://dx.doi.org/10.1016/S0304-3940\(97\)13359-6](http://dx.doi.org/10.1016/S0304-3940(97)13359-6)
- Weaver J. C., Vaughn T. E., Martin G. T. (1999): Biological effects due to weak electric and magnetic fields: the temperature variation hypothesis. *Biophys. J.* **76**, 3026–3030  
[http://dx.doi.org/10.1016/S0006-3495\(99\)77455-2](http://dx.doi.org/10.1016/S0006-3495(99)77455-2)
- Whissell P. D., Persinger M. A. (2007): Emerging synergisms between drugs and physiologically patterned weak magnetic fields: implications for neuropharmacology and the human population in the twenty-first century. *Curr. Neuropharm.* **5**, 278–288  
<http://dx.doi.org/10.2174/157015907782793603>

Received: May 3, 2013

Final version accepted: August 5, 2013